Multiscale structural anisotropy in pulvinus motor organs of the sensitive plant *Mimosa pudica*

David A. Sleboda[1,2,*], Anja Geitmann[2], and Reza Sharif-Naeini[1]

[1]Department of Physiology, McGill University

[2]Department of Plant Science, McGill University

*Corresponding Author

Present Address: David A. Sleboda, Department of Ecology and Evolutionary Biology, University of California Irvine

Abstract

Pulvini are joint-like motor organs that power active leaf movement in many plants. Multiple structural specializations spanning subcellular, cellular, and tissue scales of pulvinus organization have been described; however, the impacts of multiscale mechanics on pulvinus physiology remain poorly understood. To investigate the influence of multiscale morphology on turgor-induced deformation, we visualized *Mimosa pudica* pulvinus morphology at multiple hierarchical scales of organization and used osmotic perturbations to experimentally swell pulvini in incremental states of dissection. We observed directional cellulose microfibril reinforcement, oblong, spindle-shaped primary pit fields, and flattened, disk-like cell geometries in the parenchyma of *M. pudica*. Consistent with these observations, isolated parenchyma tissues displayed highly anisotropic swelling behaviors indicating a high degree of mechanical anisotropy. Swelling behaviors at higher scales of pulvinus organization were also influenced by the presence of the pulvinus epidermis, which displayed oblong epidermal cells oriented transverse to the pulvinus long axis. Our findings indicate that structural specializations spread across multiple hierarchical scales of organization guide hydraulic deformation of pulvini, suggesting that multiscale mechanics are crucial to the translation of cell-level turgor variations into organ-scale pulvinus motion *in vivo*.

Introduction

Pulvini are fleshy swellings located at the bases of petioles, leaves, and leaflets in many plants. They are sites of growth-independent motion and facilitate active, reversible bending of leafy plant appendages. Anatomically, pulvini are roughly cylindrical in shape and consist of a flexible core of vasculature surrounded by a thick cortex of parenchyma cells. During active deformation, bulk migration of water occurs between extensor and flexor parenchyma cell

groups located on opposing sides of the central vasculature core (Tamiya et al., 1988), resulting in a length differential between the two groups that induces long-axis pulvinus bending. Pulvinus-driven leaf folding can occur gradually over the course of hours under the influence of a circadian rhythm, or rapidly as a thigmonastic response to touch, shaking, or wounding of a plant. Active pulvinus bending is associated with efflux of K^+ and Cl^- ions from parenchyma cells (Kumon and Suda, 1984), offloading of sugar from vascular elements (Fromm and Eschrich, 1988a), and consumption of ATP (Fromm and Eschrich, 1988b), indicating that pulvinus motion is associated with active transport of ions and other osmolites to which water is attracted (Scorza and Dornelas, 2011).

While multiple theoretical models of pulvinus physiology provide insight into the biochemical mechanisms that power active movement of fluid between parenchyma cell groups (e.g. Kagawa and Saito, 2000; Morillon et al., 2001; Kwan et al., 2013; Wang and Li, 2020), relatively little is known regarding the mechanisms by which volumetric changes at the cellular level are translated into physiologically useful motion at the organ scale. Multiple morphological features have been identified which have the potential to bridge this gap. In pulvini of the scarlet runner bean *Phaseolus coccineus L.*, observations with polarized light microscopy suggest that the walls of parenchyma cells are reinforced by cellulose microfibrils oriented primarily perpendicular to the long axis of the pulvinus, confining turgor-induced cell deformation to the long axis of the organ where its effect on bending is greatest (Mayer et al., 1985). In pulvini of *Phaseolus coccineus L.* and of the common bean *Phaseolus vulgaris*, parenchyma cells are flattened in the direction parallel to the long axis of the pulvinus, displaying approximately disc-shaped morphologies that are also conducive to deformation preferentially along the long axis of the organ (Mayer et al., 1985; Koller and Zamski, 2002). In pulvini of *Albizia julibrissin*, *Phaseolus vulgaris*, and the sensitive plant *Mimosa pudica,* wrinkles in the pulvinus surface run preferentially transverse to the organ long axis and have been identified as structural features

that facilitate longitudinal deformation of the pulvinus epidermis without sacrificing circumferential stiffness (Satter et al., 1970; Koller and Zamski, 2002; Song et al., 2014; Mano and Hasebe, 2021). These structural features have the potential to physically guide hydraulic deformation of pulvini, ensuring that volumetric changes at the cellular level are ultimately translated into long-axis tissue deformations that induce macroscopic organ bending. Despite the functional importance of this role, a multiscale study surveying structural anisotropy across scales of pulvinus organization within a single plant species has not been carried out, and the distinct contributions of cell wall ultrastructure, cell geometry, and epidermis morphology to the management of hydraulic deformation remain unclear.

Here we disentangle the influences of cell wall ultrastructure, cell geometry, and epidermis morphology on turgor-induced deformation in the pulvini of *Mimosa pudica*, a touch-sensitive plant which displays both rapid thigmonastic and slow circadian leaf movements. Using a combination of scanning electron and confocal microscopy, we visualized *M. pudica* pulvinus morphology at multiple hierarchical scales of organization and characterized the degree of structural anisotropy present at each. Additionally, we used osmotic bathing solutions to experimentally swell live, isolated *M. pudica* pulvinus tissues in various states of dissection. This approach allowed us to characterize the degree of anisotropic tissue deformation that results from purely isotropic loads of intracellular fluid pressure. Differences in swelling behaviors across scales of organization are discussed in relation to the anisotropic structural features observed.

Materials and Methods

All pulvinus organs and tissue samples were harvested fresh from *Mimosa pudica* plants grown under laboratory conditions. Plants were grown from seed in a growth chamber with a 12-hour light-dark cycle at 21-23°C and 60% humidity. Plants were watered approximately once every 3 days and fertilized monthly.

Epidermis morphology

The surface morphology of the pulvinus epidermis was visualized using a Hitachi TM-1000 scanning electron microscope (SEM). Primary, secondary, and tertiary pulvini located at the bases of petioles, leaves, and leaflets, respectively, were removed from plants and dehydrated in a graded series of ethanol. Isolated pulvini were then critical point dried in liquid CO_2 and mounted in lateral view on aluminum stubs with carbon double-sided tape. Mounted organs were sputter coated with a 4 nm layer of gold and palladium and imaged at an excitation voltage of 15 kV. Aspect ratios and orientations of epidermal cells were measured manually from scanning electron micrographs of primary pulvini using ImageJ (Schindelin et al., 2012). The positions of epidermal cells along the lengths of pulvini were defined relative to their distance from the pulvinus base, measured along a path traversing the central axis of pulvinus and petiole (see yellow line depicted in fig. 2a). Total path length examined was determined by doubling the distance from the base of the pulvinus to the center of the knuckle-like protuberance immediately distal to the pulvinus (indicated as length 0.50 in fig. 2a), such that roughly equal lengths of pulvinus and petiole were examined. To facilitate comparison of pulvini of varying size, distances of epidermal cells from the pulvinus base were expressed as portions of the total path length examined for each organ. Epidermal cell orientation was measured relative to the orientation of the central path.

Cell wall ultrastructure

The ultrastructures of individual parenchymal cell walls were visualized using an environmental scanning electron microscope (FEI Quanta 450 FE-ESEM, FEI Co.) at the McGill University Facility for Electron Microscopy Research. In order to observe the inner structures of individual cell walls, primary pulvini were decellularized using an adapted protocol for the generation of acellular, cellulosic tissue engineering scaffolds from plant material (Adamski et al., 2018). Fresh pulvini were fixed overnight in 4% formaldehyde in 0.1 M phosphate buffer, pH 7.2 (Kwan et al., 2013) and then bisected longitudinally using a fine razor blade under a stereomicroscope. Fixed, bisected pulvini were immersed in an aqueous solution of 3% NaOH, 5% bleach for approximately 20 hours at room temperature until they appeared uniformly white and translucent under transmitted light illumination, indicating maceration of cellular material. Pulvini were then gently rinsed in distilled water for 24 hours, dehydrated in 100% ethanol, critical point dried in liquid CO_2, mounted on aluminum stubs with carbon double-sided tape, and sputter coated with a 4 nm layer of gold and palladium. Exposed internal faces of the bisected pulvini were imaged at an accelerating voltage of 10 kV, providing lateral views of the internal structure of the decellularized organs.

The spatial orientations of cellulose microfibrils composing parenchyma cell walls were measured from high-magnification (~50,000-65,000x) scanning electron micrographs. Cellulose microfibril orientation was quantified using the Directionality plugin in ImageJ (Liu, 1991). Analysis via either the Fourier components or local gradient modes of the plugin yielded similar results, and results from the local gradient method are reported here. Orientations of identifiable structures in each cell wall micrograph were expressed as a histogram with portion of structures observed on the Y axis and angular orientation in degrees on the X axis. The peak of a gaussian curve fit to the collective histogram compiled from all micrographs provided a quantitative metric of the predominant orientation of cellulose microfibrils across samples, and

119 the standard deviation of the gaussian curve provided a metric of histogram width, i.e., the
120 dispersion of microfibril orientations about the predominant angle.

121 Aspect ratios and spatial orientations of primary pit fields, which physically connect
122 adjacent parenchyma cells, were also measured from scanning electron micrographs manually
123 using ImageJ. Pit fields were identified as matted areas of cell wall perforated by numerous
124 plasmodesmata. The spatial orientations of both pit fields and cellulose microfibrils were
125 measured relative to the pulvinus long axis, as indicated by the orientations of nearby
126 vasculature running longitudinally through the organ core.

127 **Multiscale osmotic swelling**

128 To explore differences in osmotic swelling behaviors across scales of pulvinus
129 organization, pulvini in incremental states of dissection were imaged in aqueous mannitol baths
130 of varying tonicity. Mannitol is a biologically inert molecule and has been used previously to
131 induce osmotic deformation of pulvinus tissues (Mayer et al., 1985). Bathing in relatively dilute,
132 hypotonic mannitol solutions produces an osmotic gradient that favors movement of water into
133 cells, resulting in tissue expansion, while bathing in relatively concentrated, hypertonic mannitol
134 solutions favors movement of water out of cells, resulting in tissue shrinkage.

135 Three preparations of pulvinus organ were subjected to graded osmotic manipulation:
136 cylindrical sections of pulvini, cylindrical sections skinned of their epidermis, and isolated blocks
137 of parenchyma tissue. Cylindrical sections of pulvinus organ were produced by removing the
138 proximal and distal ends of isolated pulvini using a fine razor blade under a stereomicroscope,
139 resulting in sushi roll-like sections of pulvinus organ 1000-1500 μm long and 1000-1400 μm
140 wide. Sections comprised a core of vasculature surrounded concentrically by a thick
141 parenchyma cortex and thin enveloping epidermis. Removal of the epidermis from a subset of
142 sections was accomplished via manual skinning with a fine razor under a stereomicroscope and

143 produced cylindrical sections containing only the vasculature core and surrounding parenchyma
144 cortex. Isolated parenchyma blocks were taken from the relatively large extensor (i.e. ventral or
145 abaxial) cortexes of primary pulvini and were free of both vascular and epidermis components.
146 Flexor (i.e. dorsal or adaxial) cortexes of *M. pudica* pulvini were found to be too small to reliably
147 yield parenchyma samples via manual dissection under a stereomicroscope, and were not
148 examined in the current study.

149 Dissected pulvinus preparations were transferred through a graded series of osmotic
150 mannitol baths ranging in concentration from 0 to 878 milliosmoles (mOsm). Solution
151 concentrations were calculated and prepared via serial dilution of measured quantities of
152 mannitol dissolved in distilled water. Following an acclimation time of at least 30 minutes in each
153 osmotic bath, samples were imaged in both lateral and ventral views using a digital camera
154 (Zeiss AxioCam MRc, Carl Zeiss AG) mounted on a stereomicroscope (Zeiss SteREO
155 Discovery V8, Carl Zeiss AG). Widths, lengths, and heights of dissected pulvinus preparations
156 were measured at their maxima from stereomicrographs using ImageJ. Measurements of
157 dissected pulvinus preparations were normalized to dimensions in the most hypertonic osmotic
158 bath employed (878 mOsm). Statistically significant changes in tissue size were identified via
159 two-tailed, one sample t-tests comparing normalized dimensions in the most hypertonic (878
160 mOsm) and most hypotonic (distilled water) bathing solutions.

161 **Parenchyma cell geometry**

162 The geometries of live parenchyma cells were visualized using a laser scanning confocal
163 microscope (LSM710, Carl Zeiss AG). Thin sections of fresh parenchyma tissue were collected
164 from the relatively large extensor (i.e. ventral or abaxial) cortexes of primary pulvini using a pair
165 of razor blades spaced by ~400 μm of double-sided tape. Thin sections were prepared for
166 confocal microscopy by staining briefly (7-9 minutes) with 0.5 mg/ml propidium iodide (PI) in
167 osmotically isotonic bathing solution. PI binds to cell wall pectin and is a common stain for live

168 imaging of plant anatomical features (Bidhendi et al., 2020). Isotonic bathing tonicity was
169 determined by bathing parenchyma tissue in a graded series of aqueous mannitol solutions and
170 measuring changes in tissue size. Osmotic baths more concentrated than 384 mOsm of
171 mannitol were found to cause shrinkage of freshly dissected parenchyma tissues, while osmotic
172 baths less concentrated than 384 mOsm caused expansion. After fluorescent staining,
173 parenchyma sections were rinsed briefly of unbound PI and then excited with a 543 nm Helium-
174 Neon laser at 5% power. Fluorescence emission in a range of 554-711 nm was captured from
175 parenchyma cells deep to the sectioned tissue surface. Cells with a fluorescing nucleus
176 indicating penetration of PI into the cell protoplasm were considered damaged by sectioning and
177 excluded from the study. Optical sections 2.4-6.4 μm thick were captured at the midlines of cells
178 of interest, located by changing focus along the z-axis until the largest apparent cell dimensions
179 were presented. Slice thickness was changed by manipulating the size of the confocal pinhole.

180 To examine the influence of increased intracellular fluid volume on the geometry of
181 individual parenchyma cells, parenchyma tissues visualized via confocal microscopy were
182 initially imaged in osmotically isotonic bathing solution and subsequently re-imaged in
183 osmotically hypotonic baths of distilled water. Isotonic and hypotonic baths were exchanged
184 without moving parenchyma tissue samples from the confocal stage, allowing visualization of
185 individual parenchyma cells of interest before and after osmotic swelling. An acclimation time of
186 a least 5 minutes in hypotonic solution was given prior to re-imaging of individual cells. The
187 lengths, heights, widths, lateral perimeters, and frontal perimeters of individual parenchyma
188 cells were measured from confocal micrographs in ImageJ and normalized to dimensions in
189 osmotically isotonic baths. Changes between isotonic and hypotonic solutions were expressed
190 as percentages, and significant changes in cell dimensions between the two bath conditions
191 were identified as those significantly different from zero in a two-tailed one sample t-test. Lateral
192 aspect ratios of parenchyma cells were calculated by dividing cell length (measured in the

direction parallel to the long axis of the pulvinus) by cell height (measured along the dorsal-ventral axis of the organ). Frontal aspect ratios of cells were calculated by dividing cell width by cell height. Non-circular aspect ratios were defined as those that differed significantly from 1.0 in a two-tailed one sample t-test.

Anatomical descriptors

All anatomical descriptors employed in the current study are defined relative to organ-scale pulvinus anatomy. Lengths are measured along the long axis of the pulvinus, defined by the orientation of the vasculature tissue running longitudinally through the organ center. Heights are measured along the dorsal-ventral axis of the pulvinus, perpendicular to the neutral axis of active pulvinus bending. Widths are measured laterally across the cross-section of pulvini. These terms are employed across all hierarchical scales of organization examined. For example, the length of an individual parenchyma cell refers to size measured along the long axis of the pulvinus it composes.

Results

Pulvini of *Mimosa pudica* displayed structural anisotropy at all scales of organization examined. Epidermal cells bounding the surfaces of pulvini were oblong in shape with long axes oriented perpendicular to the organ long axis (Fig. 1). Wrinkles in the pulvinus surface were oriented predominantly transverse to the pulvinus long axis, i.e., parallel to the long axes of epidermal cells. Surface wrinkles were confined exclusively to pulvinus organs, and were not apparent on neighboring surfaces of stems, petioles, or leaflets.

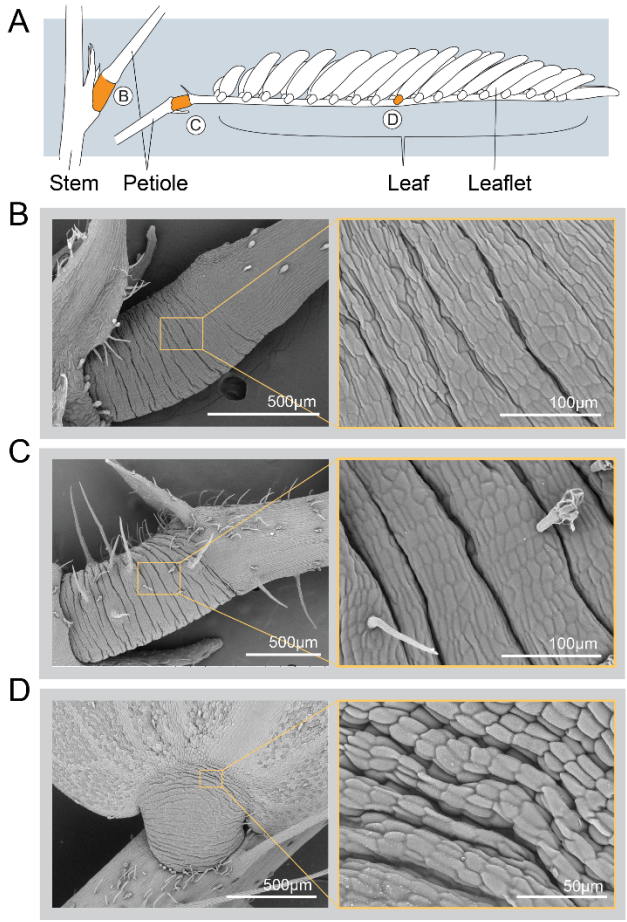

Figure 1: Pulvinus locations and external morphologies. [A] Line drawing depicting the locations of primary (B), secondary (C), and tertiary (D) pulvini of *Mimosa pudica*. [B,C,D] Scanning electron micrographs of pulvinus organs identified in A. Inset micrographs show epidermis morphology at higher magnifications. In the immediate regions of pulvini, epidermal cells are oblong and oriented perpendicular to the organ long axis. Wrinkles in the epidermis run parallel to the long axes of epidermal cells and are absent outside of the immediate regions of pulvini.

The shapes of epidermal cells of primary pulvini transitioned from oblong and perpendicularly oriented in the region of the pulvinus to oblong and parallelly oriented in the region of the petiole (Fig. 2). Epidermal cells in the intermediate region between pulvinus and petiole displayed relatively circular aspect ratios (Fig. 2b) and did not display an obvious orientation relative to the organ long axis (Fig. 2c). The average epidermal cell aspect ratio in

228 the region of the pulvinus was 3.70 ± 1.15 (mean ± SD) oriented at an average angle of 88.2° ±
229 6.85° (mean ± SD) relative to the organ long axis.

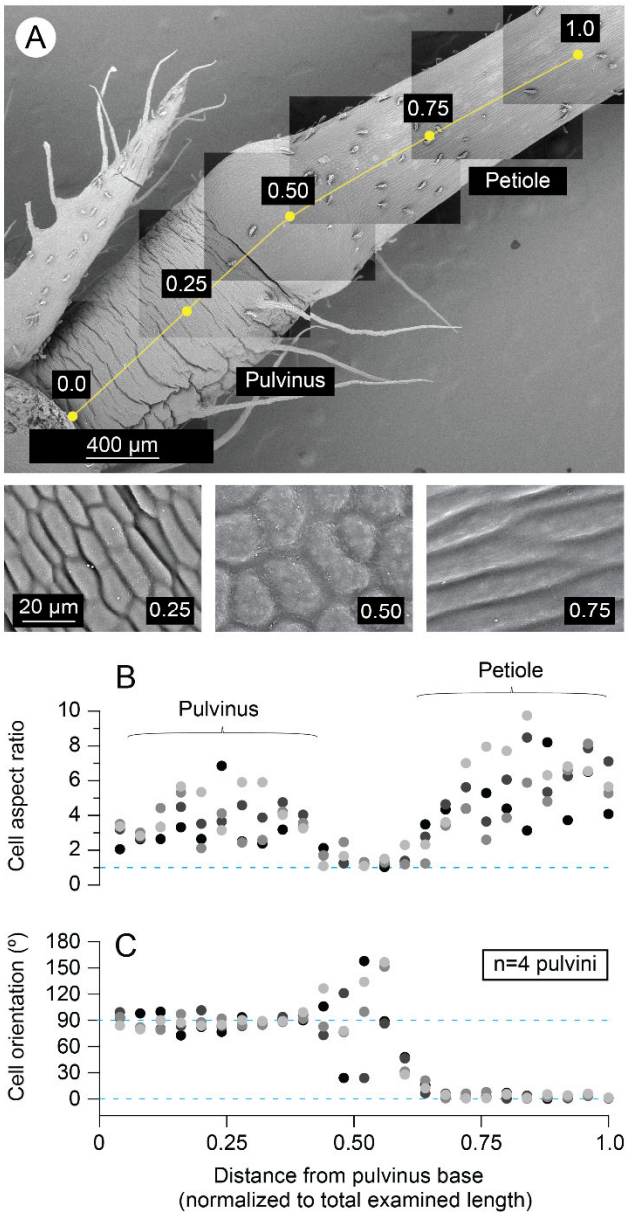

230
231
232 Figure 2: Spatial variation in epidermal cell morphology. [A] Stitched scanning electron
233 micrographs showing a primary pulvinus organ in lateral view. Yellow line depicts a path traced
234 along the central axis of pulvinus and petiole. Inset micrographs show epidermis morphology at
235 higher magnification. Labels on inset micrographs indicate the approximate location at which
236 each was taken, expressed as a portion of the total path length examined. [B] Epidermal cell
237 aspect ratio varies across the lengths of pulvini and petioles. Dashed blue line denotes a
238 circular aspect ratio of 1. [C] Epidermal cell orientations expressed relative to the orientation of
239 the central path. Dashed blue lines fall at 90° and 0° denoting perpendicular and parallel cell

240 orientations, respectively. Data points collected from the same pulvini are depicted in matching
241 shades of gray in both B and C.
242

243 High magnification scanning electron microscopy allowed visualization of individual
244 cellulose microfibrils at the inner surfaces of parenchymal cell walls (Fig. 3). Cellulose
245 microfibrils were aligned primarily dorso-ventrally in the plane of the wall with a predominant
246 microfibril orientation of 82.5° ± 29.1° (mean ± SD) relative to the orientation of nearby
247 vasculature.

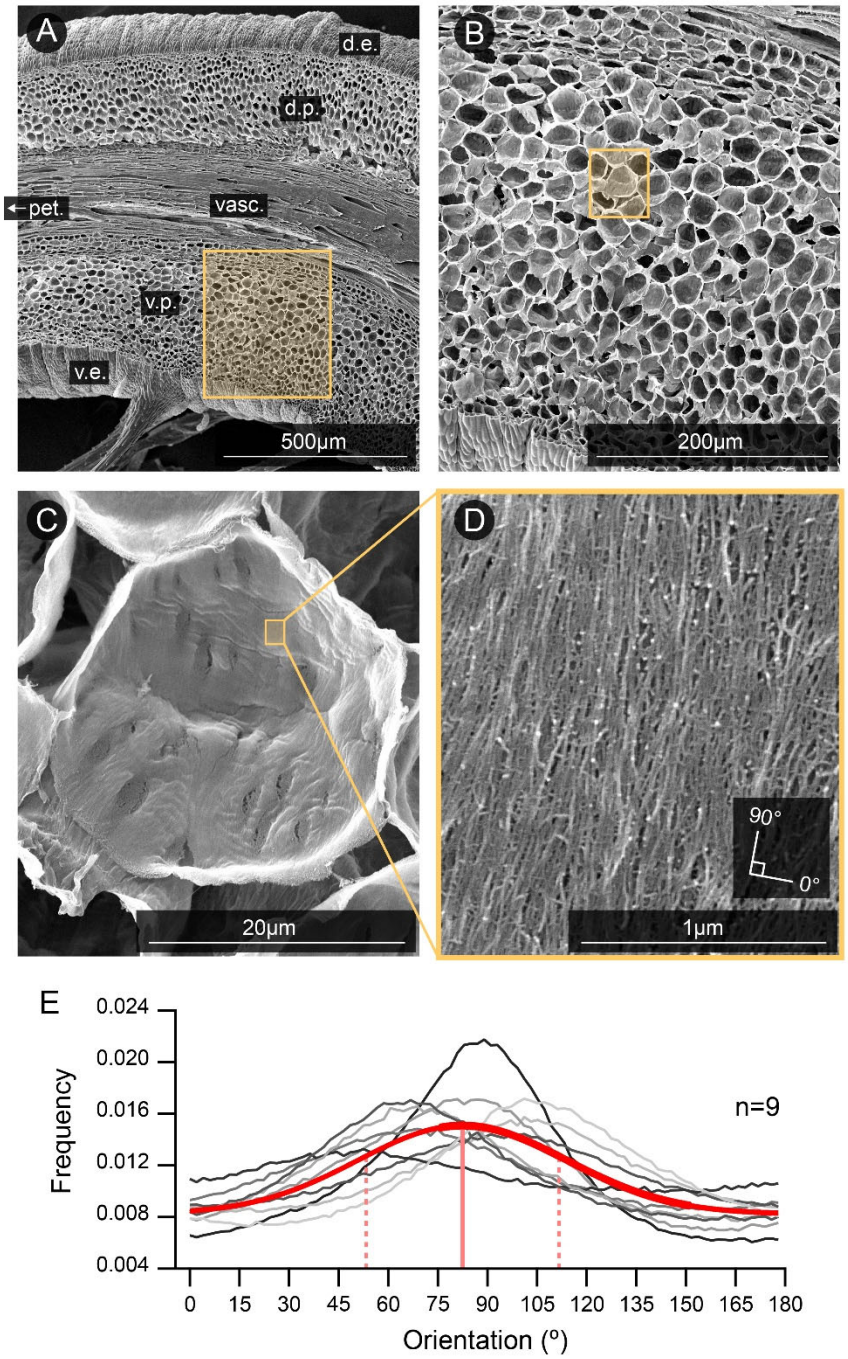

248

249 Figure 3: Orientations of cellulose microfibrils reinforcing parenchymal cell walls. [A] Scanning
250 electron micrograph showing a lateral view of a longitudinally bisected primary pulvinus.
251 Protoplasts have been removed chemically to reveal architecture at the inner face of the cell
252 wall. Labels indicate dorsal, i.e. adaxial, epidermis (d.e.), dorsal parenchyma (d.p.), vasculature
253 (vasc.), ventral, i.e. abaxial, parenchyma (v.p.), and ventral epidermis (v.e.). Organ is oriented
254 with petiole (pet.; not visible) left of the frame. [B] Magnified view of the highlighted region in A
255 showing ventral parenchyma bounded by vasculature and ventral epidermis. [C] Magnified view
256 of the highlighted region in B showing the inner face of one parenchymal cell wall. [D] High

magnification view of the highlighted region in C showing cellulose microfibrils running primarily dorso-ventrally in the plane of the cell wall. Fiber angles are described relative to the long axis of nearby vasculature (defined as 0°) with 90° indicating a perpendicular orientation. [E] Histograms showing distributions of fiber orientations in 9 cells from 4 pulvini. Each gray trace shows the distribution of fiber angles in a high magnification scanning electron micrograph similar to D. A gaussian curve (solid red trace) fit to all histograms indicates a predominant fiber orientation of 82.5 degrees (solid vertical line) with a standard deviation of ± 29.1 degrees (dotted vertical lines).

Consistent with the necessity for rapid fluid exchange during active movement, primary pit fields connecting adjacent parenchyma cells were prevalent in pulvini of *M. pudica*. Pit fields displayed a mix of circular, oval, and spindle-shaped morphologies (Fig. 4). In many parenchyma cells, pit fields were predominantly oval or spindle-shaped with long axes oriented perpendicular to the organ axis. For example, pit fields in the five parenchyma cells depicted in figure 4b displayed aspect ratios ranging from 1.2 to 4 with an average aspect ratio of 2.22 ± 0.78 (mean ± SD, n=30 pit fields) and an average long axis orientation of 93.0 ± 25.0 degrees (mean ± SD) relative to the organ axis. Parenchyma cells with predominantly oval or spindle-shaped pit fields were often directly adjacent to cells with predominantly circular pit fields, indicating that parenchyma cells of similar size, shape, and position can possess pit fields of varying morphology.

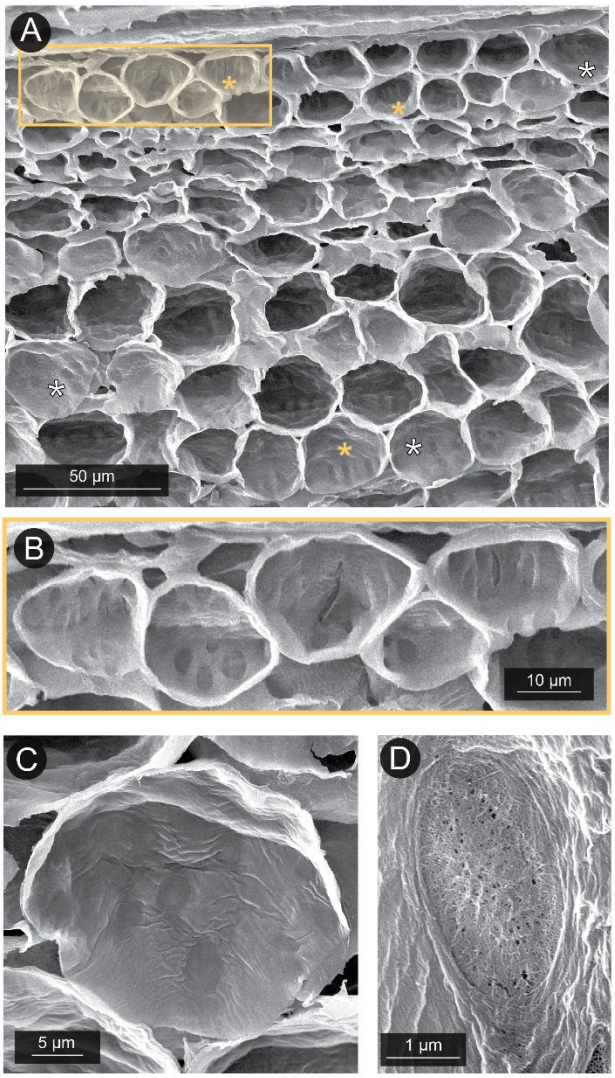

Figure 4: Primary pit fields visible in the walls of decellularized parenchyma cells. [A] Scanning electron micrograph showing a lateral view of a longitudinally bisected primary pulvinus. The organ long axis is oriented horizontally with the central vascular core visible at the top of the panel. Pit fields are visible as darkened regions of cell wall and display a mix of circular, oval, and spindle-shaped morphologies. Yellow asterisks highlight cells displaying predominantly oblong pit fields oriented perpendicular to the long axis of the pulvinus. White asterisks highlight cells with more circular pit field morphologies. [B] Magnified view of the highlighted region in A showing parenchyma cells with predominantly spindle-shaped pit fields oriented perpendicular to the organ long axis. [C] A single parenchyma cell displaying a mix of circular and oval shaped pit fields. [D] A single spindle-shaped pit field composed of mat-like cellulose microfibrils perforated by numerous plasmodesmata channels.

Osmotic swelling of dissected pulvinus organs and tissue samples yielded anisotropic deformation across all scales of pulvinus organization studied (Fig. 5). Across a graded series of osmotic baths ranging from 0 to 878 mOsm, cylindrical sections of pulvinus organ with an intact epidermis (Fig. 5c) displayed a 15.3 ± 2.75% (mean ± SD, $p < 0.01$) change in length without significant changes in either width (1.74 ± 1.83%, $p = 0.11$) or height (1.02 ± 2.42%, $p= 0.10$). Cylindrical pulvinus sections skinned of their epidermis (Fig. 5d) varied in length 17.7 ± 4.26% ($p < 0.01$), increased marginally in width (2.91 ± 1.98%, $p < 0.01$), and displayed increased variation in height (7.80 ± 8.55%, $p = 0.05$). The increased variation in the height of cylindrical organ sections skinned of their epidermis was attributable to a tendency for elongating parenchyma tissues to bow dorsally and ventrally away from the central vasculature of the pulvinus organ. This bowing resulted in skinned pulvinus sections adopting spindle-shaped lateral profiles reminiscent of rugby or American footballs when swollen osmotically (Fig. 5f). Isolated blocks of parenchyma tissue dissected free of epidermis and vasculature (Fig. 5e) changed in length 26.2 ± 3.15% ($p < 0.01$) without statistically significant changes in either width (-1.39 ± 2.40%, $p = 0.26$) or height (3.76 ± 5.75%, $p = 0.22$).

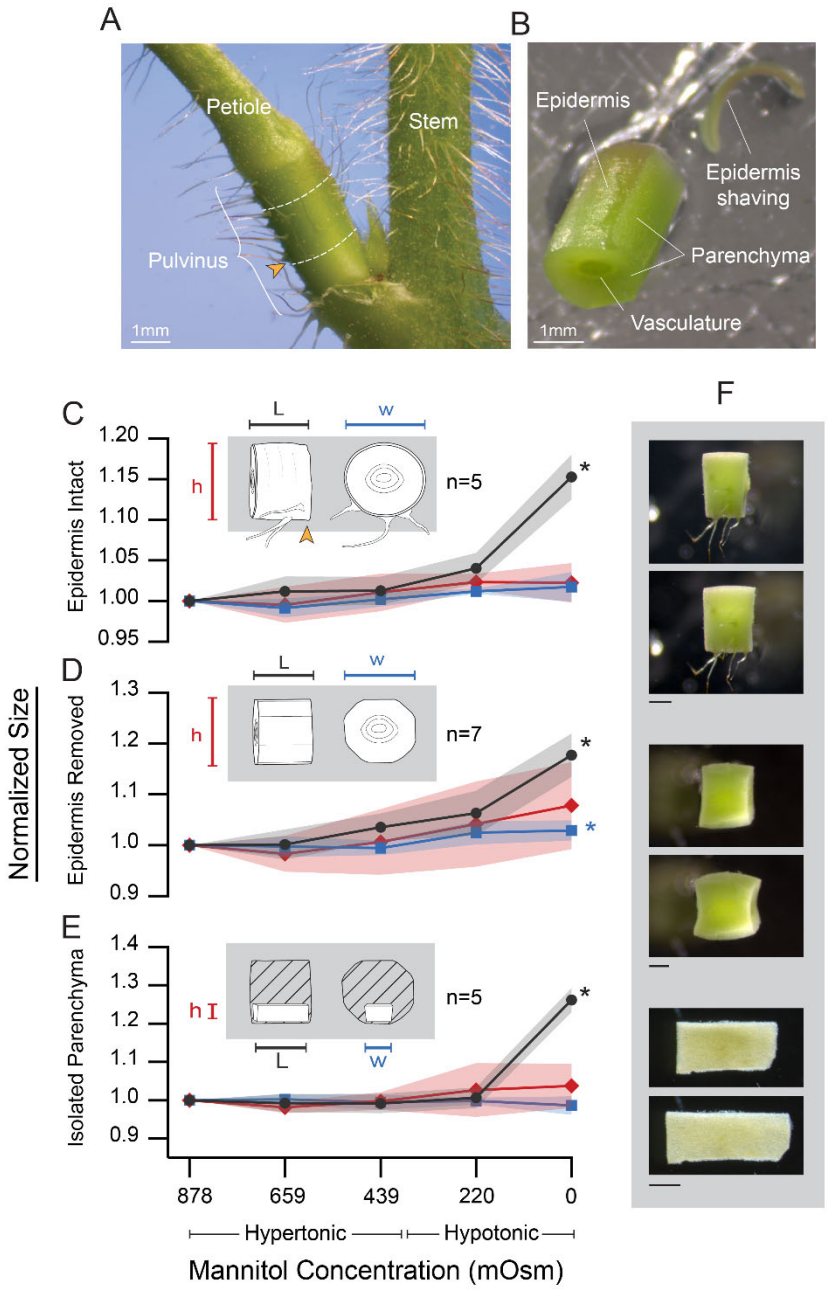

Figure 5: Osmotic perturbations reveal anisotropic swelling behaviors across scales of organization. [A] Lateral view of an intact *Mimosa pudica* primary pulvinus with flanking leaves removed. Dashed white lines illustrate cross-sectional cuts used to isolate a cylindrical section of pulvinus. Orange arrowheads in A and C indicate proximal, ventral corner of sections. [B] Isolated cylindrical section of pulvinus with epidermis partially removed to illustrate skinning technique. [C, D, E] Effect of graded osmotic bathing solutions on the length (L, black circles), cross-sectional width (w, blue squares), and height (h, red diamonds) of excised pulvinus sections. Inset line drawings depict dimensions and typical morphologies in lateral and cross-sectional views. Graph markers are means ± SD. Data is normalized to tissue dimensions in the most hypertonic bathing solution (878 mOsm). Asterisks denote values significantly different

317 from 1.0 in the most hypotonic bathing solution (0 mOsm). [C] Isolated pulvinus sections expand
318 longitudinally in increasingly hypotonic bathing solutions with negligible change in width or
319 height. [D] Sections manually skinned of their epidermis expand primarily in length but display a
320 small increase in width and increased variability in height. [E] Isolated blocks of parenchyma
321 tissue expand longitudinally with negligible change in width or height. Sample sizes (n) for each
322 condition are noted beside inset illustrations. [F] Representative images illustrating shape
323 changes of pulvinus preparations. Upper and lower images of each pair display sample shape in
324 hypertonic and hypotonic baths, respectively. Scale bars 500 μm.

325

326 The geometries of live parenchyma cells visualized by confocal microscopy depended
327 on the tonicity of the solution in which they were bathed (Fig. 6). In isotonic bathing solution, the
328 average ratio of cell width to cell height was 0.95 ± 0.15 (mean ± SD), which does not differ
329 significantly from a circular cross-sectional aspect ratio of 1.0 ($p=0.54$). The average ratio of cell
330 length to cell height was 0.85 ± 0.27 (mean ± SD), which differs significantly from a circular
331 lateral aspect ratio of 1.0 ($p=0.01$), confirming that live parenchyma cells bathed in isotonic
332 solution are approximately disk-shaped; circular in cross section but flattened longitudinally in
333 the direction parallel to the long axis of the pulvinus. Cells reimaged in osmotically hypotonic
334 distilled water baths did not change significantly in width (-0.56 ± 1.88%, mean ± SD, $p = 0.13$),
335 displayed a small but significant change in height (1.78 ± 2.99%, $p < 0.01$), and displayed a
336 relatively large increase in length of 14.5 ± 5.07% ($p < 0.01$) occurring along the long axis of the
337 pulvinus (Fig. 6b). Following transfer to hypotonic bathing solution, cells displayed an average
338 ratio of cell length to cell height of 0.96 ± 0.30, which was not significantly different from circular
339 ($p=0.54$), indicating that longitudinally flattened, disk-shaped cells expanded towards more
340 perfectly circular lateral profiles under increased turgor.

341 Measurements of frontal and lateral cell perimeters revealed anisotropy in the amount of
342 cell wall distension that occurred during osmotic expansion. Lateral cell perimeter, measured in
343 the plane parallel to the organ long axis, increased 6.87 ± 3.10% ($p < 0.01$) following
344 acclimation in hypotonic bathing solution. In contrast, frontal cell perimeter measured in cross
345 section perpendicular to the organ long axis changed only marginally (0.96 ± 1.41%, $p < 0.01$).

346 This difference in cell wall distension under isotropic turgor rise indicates that the parenchyma
347 cell wall is materially anisotropic, displaying greater extensibility in the longitudinal direction than
348 in the circumferential.

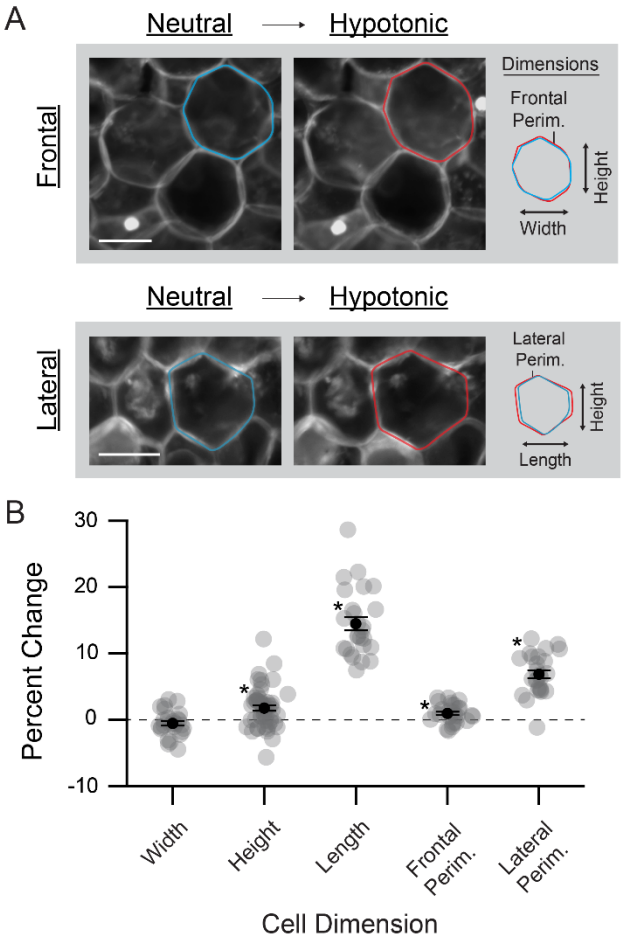

349

350 Figure 6: Nonuniform osmotic swelling of individual parenchyma cells. [A] Confocal micrographs
351 of parenchyma tissue imaged in osmotically isotonic (384 mOsm) and hypotonic (distilled water)
352 baths. Representative micrographs show cell morphology as seen in frontal and lateral views.
353 All scale bars 20 μm. Inset line drawings illustrate anatomical dimensions and highlight changes
354 in cell shape between osmotic baths. [B] Effect of osmotic swelling on frontal and lateral
355 dimensions of 53 cells from 8 pulvini. Gray dots represent percent changes in cell dimensions
356 following transfer from isotonic to hypotonic bath. Black markers represent means ± standard
357 errors. Asterisks denote percent changes significantly different from zero ($p<0.05$).

358

359 **Discussion**

360 The hydraulic nature of pulvinus-driven movement has been recognized since the 1800s
361 and is discussed in Darwin's *The Power of Movement in Plants* (Darwin and Darwin, 1880).
362 However, an understanding of the functional morphologies that transform isotropic cellular
363 turgor pressures into anisotropic, directed movement at the organ scale has remained
364 fragmented. Here we demonstrate that in pulvini of *Mimosa pudica,* multiple anisotropic
365 structural features are present across subcellular, cellular, and tissue levels of organization.
366 These include perpendicularly oriented cellulose microfibrils and primary pit fields in
367 parenchymal cell walls, longitudinally flattened parenchyma cell geometries, and perpendicularly
368 oriented epidermal cells associated with transverse surface wrinkles. We observed highly
369 anisotropic osmotic swelling of parenchyma cells and tissues; however, swelling behaviors at
370 higher levels of organization were also influenced by the presence of the enveloping epidermis,
371 suggesting that hydraulic deformation of pulvini is influenced by structural anisotropy at multiple
372 hierarchical scales.

373 **Cell wall anisotropy**

374 Consistent with polarized light investigations of pulvinus morphology in the scarlet runner
375 bean *Phaseolus coccineus L* (Mayer et al., 1985), scanning electron micrographs of
376 decellularized *M. pudica* pulvini revealed cellulose microfibrils oriented predominantly
377 perpendicular to the long axes of pulvini. Cellulose microfibrils are crystalline structures
378 composed of closely packed chains of parallelly-oriented cellulose molecules (Brett, 2000) and
379 display high tensile strengths and longitudinal stiffnesses of approximately 1 GPa and 130 GPa
380 respectively (Gibson, 2012). Cellulose microfibrils function as the primary mechanical
381 component of the plant cell wall, ultimately providing the tensile strength needed to balance
382 large intracellular turgor pressures ranging from 0.4-0.8 MPa in typical hydrated plant tissues
383 (Taiz et al., 2015) to over 1 MPa in some specialized plant cells (Franks, 2003).

384 Anisotropic patterns of cellulose reinforcement are not unique to pulvini. Cellulose
385 orientation is actively controlled by the microtubule-guided motion of cellulose synthase
386 complexes that extrude cellulose microfibrils into the extracellular space (Brett, 2000), and
387 anisotropic cellulose deposition is the primary means by which mechanical anisotropy is
388 produced and maintained in plant cell walls. The interplay of intracellular turgor pressure and
389 cell wall anisotropy ultimately governs the direction of irreversible turgor induced shape changes
390 (Baskin, 2005) and underlies the development of complex non-spherical morphologies
391 (Bidhendi and Geitmann, 2016) in growing plant cells. Interactions between cell wall anisotropy
392 and turgor pressure have also been shown to underlie reversible deformation of certain mature
393 plant cell types. The hydraulic guard cells flanking stomatal pores, for example, are reinforced
394 by cellulose microfibrils oriented primarily perpendicular to the guard cell long axes (Galatis and
395 Apostolakos, 2004). The perpendicular orientation of microfibrils inhibits radial expansion of
396 guard cells while permitting elongation during hydraulic expansion, ultimately facilitating the
397 microscopic outward bowing of guard cells that facilitates repeated opening and closing of
398 stomatal pores (Aylor et al., 1973). Parenchyma cells observed in the current study displayed a
399 high degree of directional anisotropy in the extensibilities of their cell walls, with osmotic
400 expansion causing wall distension approximately 7 times greater in the longitudinal direction
401 than in the circumferential. Analogous to the effect of cellulose anisotropy in stomatal guard
402 cells, this finding suggests that cellulose microfibrils selectively restrict circumferential
403 expansion of parenchymal cell walls in the pulvini of *M. pudica*, resulting in predominantly
404 longitudinal cell wall deformation in response to turgor change.

405 In addition to unidirectionally oriented cellulose microfibrils, frequent primary pit fields
406 also have the potential to contribute to mechanical anisotropy in the parenchyma cell wall.
407 Primary pit fields are typically circular, sometimes oval regions of the primary cell wall perforated
408 by numerous plasmodesmata. In addition to being perforated, the cell wall is significantly thinner

409 in pit fields compared to the surrounding wall, commonly by a factor of 5 or more (e.g. Kobiyama
410 and Crandall-Stotler, 1999). The presence of numerous primary pit fields is consistent with the
411 importance of rapid water exchange between cells in the *M. pudica* pulvinus; however, the
412 presence of many oblong and spindle-shaped pit fields oriented perpendicular to the organ axis
413 suggests their shape and orientation may also serve a mechanical function. Assuming the
414 reduced thickness of the pit field is associated with a lower elastic modulus, oblong pit fields
415 oriented perpendicular to the pulvinus axis may serve as expandable seams that facilitate
416 distension of the cell wall preferentially in the longitudinal direction. Direct measurements of pit
417 field deformation or elastic modulus are needed to verify this hypothesis, and exploration of the
418 influence of pit field material properties and shape on cell wall mechanics may prove a fruitful
419 topic for future research.

420 **Geometric deformation of parenchyma cells**

421 While perpendicularly oriented cellulose microfibrils and pit fields are conducive to long-
422 axis deformation of parenchyma cells, our results indicate that direct stretching of the cell wall
423 cannot account for all of the longitudinal cell deformation observed in the current study.
424 Following transfer from isotonic to hypotonic bathing solution, the average length of parenchyma
425 cells increased by 14.5 ± 5.07% (mean ± SD); however, the lateral perimeters of these same
426 parenchyma cells increased by only 6.87 ± 3.10%, indicating that direct stretching of the cell
427 wall accounts for less than half of longitudinal cell deformation on average, even under the
428 assumption that all cell wall distension contributes exclusively to elongation. Geometric
429 deformation of cells from longitudinally flattened lateral profiles towards more longitudinally
430 expanded lateral profiles likely accounts for the remaining observed cell deformation. Like the
431 corrugated bellows of an accordion or concertina, the longitudinally flattened morphologies of
432 parenchyma cells are conducive to longitudinal expansion and contraction via geometric
433 changes in cell shape. We observed both direct distension of the cell wall and geometric shape

434 changes of cells under increased turgor, indicating that both of these mechanisms contributed to
435 anisotropic parenchyma cell deformation during experimentally imposed swelling. Further
436 studies of parenchyma cell deformation at physiologically realistic intracellular turgor pressures
437 are needed to determine the relative contributions of these two mechanisms to anisotropic
438 deformation *in vivo*.

439 Here we focus exclusively on parenchyma cells from the relatively large extensor (i.e.
440 ventral or abaxial) cortex of the primary pulvinus of *M. pudica*. Comparison with morphology and
441 swelling behavior of the flexor cortex was not carried out in the current study but is a worthwhile
442 topic for future research. We expect that parenchyma cells of the flexor cortex would display
443 similar structural anisotropy and directional swelling behavior to that of the extensor cortex;
444 however, subtle differences in morphology across cortexes likely influence their behaviors. In
445 pulvini of the scarlet runner bean *Phaseolus coccineus L.,* for example, both extensor and flexor
446 cortexes are composed of longitudinally flattened, disk-like parenchyma cells. Cells of the
447 extensor compartment are notably larger in size, and isolated blocks of extensor parenchyma
448 tissue display relatively larger percent changes in length than flexor tissues when osmotically
449 swollen in distilled water (Mayer et al. 1985). Such differences may be relevant to pulvinus
450 mechanics *in vivo*, and further investigation may provide insight into the granularity of
451 morphological specialization displayed by parenchyma cells that are subject to differing
452 functional demands.

453 **Mechanical contribution of the pulvinus epidermis**

454 Most plant stems and petioles are ensheathed in a skin of elongate epidermal cells
455 oriented parallel to the long axis of the organ (Kutschera, 2008). This parallel orientation of
456 epidermal cells is a natural consequence of turgor-driven morphogenesis, in which elongated
457 plant organs form developmentally through anisotropic expansion and elongation of the cells
458 that compose them. Over most of their lengths, the petioles of *M. pudica* display a typical

459 epidermis morphology of elongate cells oriented parallel to the organ long axis. Surprisingly,
460 however, we observed epidermal cells oriented perpendicular to the growth axis in the
461 immediate regions of pulvini. Perpendicular cells correlated spatially with the presence of
462 transverse wrinkles oriented perpendicular to the long axis of the pulvinus. Transverse wrinkles
463 in the epidermis of *Mimosa pudica* have been described previously and have been shown to
464 expand and contract dynamically during active movement of live plants (Song et al., 2014).
465 They are thought to provide extra surface area that increases the longitudinal extensibility of the
466 epidermis without compromising its circumferential stiffness (Mano and Hasebe, 2021).

467 We suggest that perpendicularly oriented epidermal cells are a morphological
468 specialization that facilitates transverse wrinkling of the epidermis by reducing its effective
469 flexural stiffness in the longitudinal direction. Epidermal cell orientation has been shown to have
470 a direct effect on the material stiffness of plant epidermis, inducing anisotropic tensile properties
471 and relatively lower tensile stiffness in the direction perpendicular to the orientation of epidermal
472 cells (Bidhendi et al. 2020). Importantly, a perpendicular orientation of epidermal cells also
473 allows transverse wrinkles to form between epidermal cells rather than across their lengths,
474 minimizing bending strains imposed on individual epidermal cells. Direct mechanical tests
475 exploring the impact of epidermal cell orientation on flexural stiffness are needed; however,
476 facilitation of transverse wrinkle formation provides a potential explanation for the observation of
477 perpendicularly oriented epidermal cells confined to the immediate regions of pulvini.

478 In cylindrical sections of pulvinus organ skinned of an enveloping epidermis, we
479 observed outward bowing of parenchyma tissue away from the central axis of cylindrical
480 pulvinus sections during osmotic swelling. We suspect that this parenchymal bowing results
481 from a difference in the longitudinal extensibility of parenchyma tissues and the vascular tissue
482 they surround. Isolated parenchyma tissues dissected away from the mechanical context of the
483 pulvinus organ display a strong bias for purely longitudinal expansion; however, when coupled

484 to a relatively stiff vasculature core in the context of an intact organ, pure longitudinal expansion
485 of the parenchyma along a straight line is resisted, and outward curvature of longitudinally
486 expanding parenchyma tissues results. We did not observe the phenomenon of outward
487 parenchyma bowing in pulvinus preparations with an intact epidermis, suggesting that the
488 circumferential stiffness of the epidermis resists outward bowing of parenchyma tissues. While
489 anisotropic cell wall reinforcement and cell geometry are well suited to ensure longitudinal
490 expansion at the scale of individual parenchyma cells, our findings suggest that the transversely
491 wrinkled epidermis serves as an encompassing sleeve that restricts radial deformations that
492 emerge at higher scales of tissue organization, ensuring that hydraulic expansion of
493 parenchyma tissue *en masse* remains aligned along the long axis of the pulvinus where its
494 effect on organ bending is greatest.

495 **Osmotic swelling as a model for *in vivo* physiology**

496 Simple osmotic swelling and shrinkage of pulvinus tissues does not replicate the rapid
497 and complex mechanisms of intercellular fluid movement employed by *Mimosa pudica* pulvini *in*
498 *vivo*, the details of which are not fully understood. Rather, osmotic perturbations employed in
499 the current study provide a means of introducing purely isotropic, nondirectional intracellular
500 loads into parenchyma cells in the form of hydrostatic fluid pressures, the effects of which
501 provide insight into multiscale tissue mechanics. While the precise physiological mechanisms
502 powering active fluid movement and turgor change *in vivo* is an important topic for further
503 investigation, here we show that hydraulic deformation of *M. pudica* pulvini is a product not only
504 of biochemical specialization, but also of a suite of downstream structural features that span
505 multiple hierarchical scales of organization. These features are ideally situated to translate
506 isotropic, non-directional cellular turgor pressures into the physiologically relevant motor task of
507 long-axis organ bending, suggesting that they are important contributors to the mechanism of
508 pulvinus-driven motion *in vivo*.

Acknowledgements

We thank Youssef Chebli for help in microscope operation and helpful discussions about data collection, and David Liu and S. Kelly Sears at the Facility for Electron Microscopy Research of McGill University for help in microscope operation and data collection.

Funding

Funded by a Human Frontier Science Program long-term postdoctoral fellowship (LT - 000531/ 2020).

Competing Interests

We have no competing interests to declare.

Data availability

Tabulated data from all figures are available as supplemental files.

References Cited

Adamski, M., Fontana, G., Gershlak, J. R., Gaudette, G. R., Le, H. D. and Murphy, W. L. (2018). Two methods for decellularization of plant tissues for tissue engineering applications. *J. Vis. Exp.*, 135, e57586. 10.3791/57586.

Aylor, D. E., Parlange, J. Y. and Krikorian, A. D. (1973). Stomatal mechanics. *Am. J. Bot., 60*(2), 163-171. 10.1002/j.1537-2197.1973.tb10213.x.

Baskin, T. I. (2005). Anisotropic expansion of the plant cell wall. *Annu. Rev. Cell Dev. Biol., 21*, 203-222. 10.1146/annurev.cellbio.20.082503.103053.

Bidhendi, A. J., Chebli, Y. and Geitmann, A. (2020). Fluorescence visualization of cellulose and pectin in the primary plant cell wall. *J. Microsc., 278*(3), 164-181. 10.1111/jmi.12895.

Bidhendi, A. J. and Geitmann, A. (2016). Relating the mechanics of the primary plant cell wall to morphogenesis. *J. Exp. Bot., 67*(2), 449-461. 10.1093/jxb/erv535.

Bidhendi, A. J., Li, H. and Geitmann, A. (2020). Modeling the nonlinear elastic behavior of plant epidermis. *Botany, 98*(1), 49-64. 10.1139/cjb-2019-0058.

Brett, C. T. (2000). Cellulose microfibrils in plants: biosynthesis, deposition, and integration into the cell wall. *Int. Rev. Cytol.,* 199, 161-199. 10.1016/S0074-7696(00)99004-1.

Darwin, C. and Darwin, F. (1880). *The power of movement in plants*. Appleton, New York, NY.

Franks, P. J. (2003). Use of the pressure probe in studies of stomatal function. *J. Exp. Bot., 54*(387), 1495-1504. 10.1093/jxb/erg162.

Fromm, J. and Eschrich, W. (1988a). Transport processes in stimulated and non-stimulated leaves of *Mimosa pudica*. *Trees, 2*(1), 7-17. 10.1007/BF00196974.

Fromm, J. and Eschrich, W. (1988b). Transport processes in stimulated and non-stimulated leaves of *Mimosa pudica*. *Trees, 2*(1), 18-24. 10.1007/BF00196975.

Galatis, B. and Apostolakos, P. (2004). The role of the cytoskeleton in the morphogenesis and function of stomatal complexes. *New Phytol., 161*(3), 613-639. 10.1046/j.1469-8137.2003.00986.x.

Gibson, L. J. (2012). The hierarchical structure and mechanics of plant materials. *J. R. Soc. Interface, 9*(76), 2749-2766. 10.1098/rsif.2012.0341.

Kagawa, H. and Saito, E. (2000). A model on the main pulvinus movement of *Mimosa pudica*. *JSME Int. J. C-Mech Sy., 43*(4), 923-928. 10.1299/jsmec.43.923.

Kobiyama, Y. and Crandall-Stotler, B. (1999) Studies of specialized pitted parenchyma cells of the liverwort *Conocephalum* Hill and their phylogenetic implications. *Int. J. Plant Sci.*, 160(2), 351-370. 10.1086/314126.

Koller, D. and Zamski, E. (2002). The phototropic pulvinus of bean *Phaseolus vulgaris L*.-Functional features. *Plant Biol., 4*(5), 584-594. 10.1055/s-2002-35442.

Kumon, K. and Suda, S. (1984). Ionic Fluxes from Pulvinar Cells during the Rapid Movement of *Mimosa pudica L. Plant. Cell. Physiol., 25*(6), 975-979. 10.1093/oxfordjournals.pcp.a076813.

Kutschera, U. (2008). The growing outer epidermal wall: design and physiological role of a composite structure. *Ann. Bot., 101*(5), 615-621. 10.1093/aob/mcn015.

Kwan, K., Ye, Z., Chye, M. and Ngan, A. (2013). A mathematical model on water redistribution mechanism of the seismonastic movement of *Mimosa pudica*. *Biophys. J., 105*(1), 266-275. 10.1016/j.bpj.2013.06.001.

Liu, Z. Q. (1991). Scale space approach to directional analysis of images. *Appl. Opt., 30*(11), 1369-1373. 10.1364/AO.30.001369.

Mano, H. and Hasebe, M. (2021). Rapid movements in plants. *J. Plant. Res., 134*(1), 3-17. 10.1007/s10265-020-01243-7.

Mayer, W.-E., Flach, D., Raju, M., Starrach, N. and Wiech, E. (1985). Mechanics of circadian pulvini movements in *Phaseolus coccineus L*. *Planta, 163*(3), 381-390. 10.1007/BF00395147.

Morillon, R., Liénard, D., Chrispeels, M. J. and Lassalles, J.-P. (2001). Rapid movements of plants organs require solute-water cotransporters or contractile proteins. *Plant Physiol., 127*(3), 720-723. 10.1104/pp.010732.

Satter, R. L., Sabnis, D. D. and Galston, A. W. (1970). Phytochrome controlled nyctinasty in *Albizzia julibrissin*. I. Anatomy and fine structure of the pulvinule. *Am. J. Bot., 57*(4), 374-381. 10.1002/j.1537-2197.1970.tb09826.x.

581 Schindelin, J., Arganda-Carreras, I., Frise, E., Kaynig, V., Longair, M., Pietzsch, T., Preibisch,
582 S., Rueden, C., Saalfeld, S., Schmid, B., Tinevez, J. Y., White, D. J., Hartenstein, V.,
583 Eliceiri, K., Tomancak, P. and Cardona, A. (2012). Fiji: an open-source platform for
584 biological-image analysis. *Nat. Methods, 9*(7), 676-682. 10.1038/nmeth.2019.
585 Scorza, L. C. T. and Dornelas, M. C. (2011). Plants on the move: towards common mechanisms
586 governing mechanically-induced plant movements. *Plant Signal. Behav., 6*(12), 1979-
587 1986. 10.4161/psb.6.12.18192.
588 Song, K., Yeom, E. and Lee, S. J. (2014). Real-time imaging of pulvinus bending *in Mimosa*
589 *pudica*. *Sci. Rep., 4*, 6466. 10.1038/srep06466.
590 Taiz, L., Zeiger, E., Møller, I. M. and Murphy, A. (2015). *Plant physiology and development*:
591 Sinauer Associates, Sunderland, CT.
592 Tamiya, T., Miyazaki, T., Ishikawa, H., Iriguchi, N., Maki, T., Matsumoto, J. J. and Tsuchiya, T.
593 (1988). Movement of water in conjunction with plant movement visualized by NMR
594 imaging. *J. Biochem., 104*(1), 5-8. 10.1093/oxfordjournals.jbchem.a122421.
595 Wang, Y. and Li, H. (2020). Bio-chemo-electro-mechanical modelling of the rapid movement of
596 Mimosa pudica. *Bioelectrochemistry, 134*, 107533. 10.1016/j.bioelechem.2020.107533.